

Applicability and Limitations of an *M2Spice*-assisted “Planar-Magnetics-in-the-Circuit” Simulation Approach

Samantha J. Gunter¹, Minjie Chen¹, Stephanie A. Pavlick¹, Rose A. Abramson¹,
Khurram K. Afridi², and David J. Perreault¹

¹Massachusetts Institute of Technology, Cambridge, MA, 02139, USA

²University of Colorado Boulder, Boulder, CO, 80309, USA

Abstract—Planar magnetics design for power electronics naturally involves many tradeoffs, especially in the selection of the core size, winding structure and printed circuit board stackup. “Magnetics-in-the-circuit” SPICE simulations can facilitate quick magnetics design evaluation and iteration. This paper introduces and evaluates a “planar-magnetics-in-the-circuit” simulation approach with an *M2Spice* software tool, which has been developed based on an earlier presented Modular Layer Model (MLM) analysis approach [1]. *M2Spice* converts the magnetics geometry into a SPICE netlist, which can be simulated with other circuit elements in a power converter under a unified setup. This paper presents an analysis of the applicability and limitations of this approach across wide frequency bands, followed by an evaluation of the accuracy of the SPICE simulation results (by comparing the simulation results to finite-element-modeling (FEM) results and experimental measurements). Multiple planar magnetics prototypes are designed, modeled, simulated, built, and measured, with results reported and discussed.

Index Terms—planar magnetics, lumped circuit model, 1-D methods, time-domain simulation.

I. INTRODUCTION

PLANAR magnetics offer low profile, good thermal characteristics, high power density, high repeatability and the ease of realizing complex winding structures [2]–[4]. As frequency increases, accurate modeling of planar magnetics becomes both important and increasingly challenging, mostly due to the impact of skin- and proximity-effects. In previous work, efforts have been made to estimate the loss [5]–[9], extract parasitics [10], and investigate the current distribution in windings [11]–[20]. Numerical methods (e.g., finite-element-modeling) and discretization-based experimental measurements are widely applicable, but are often difficult to use for design optimizations that involve many tradeoffs.

Following earlier modeling work that utilizes modularized sub-circuit cells to represent planar layers [12]–[20], an analytical model, named the Modular Layer Model (MLM), that is widely applicable to modeling planar magnetics, has been recently presented in [1]. The MLM is developed based on a minimum set of assumptions - the 1-D and the magneto-quasistatic (MQS) assumptions. It utilizes analytical solutions for field and current relationships and captures the relationship between variables in the electromagnetic domain and variables in the circuit domain using KVL and KCL equations. The current distribution and field strength can be rapidly found

S. Gunter and M. Chen have equal contribution to this paper.

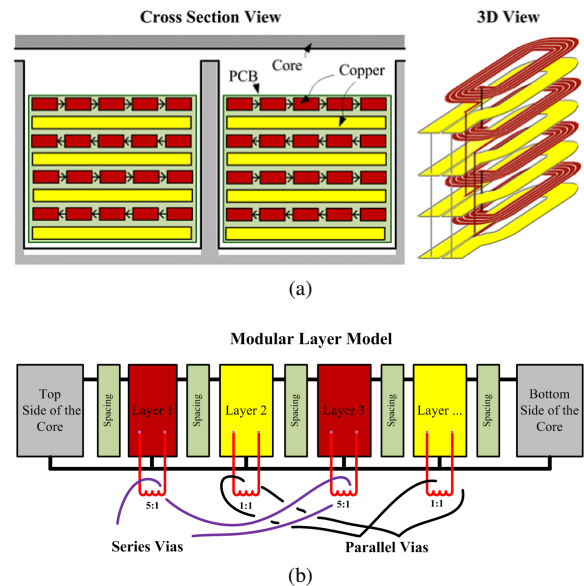


Fig. 1. Modular Layer Model-based modeling approach presented in [1]. (a) Physical structure consisting of many layers. (b) The full structure broken into many sub-sections.

using SPICE simulations, and be visualized in the time-domain when the magnetic device is connected to an external circuit.

With additional assumptions and approximations, “1-D-single-frequency” magnetic models can be extended to cover 2-D or wide-frequency-band cases by curve-fitting methods (linearization), or discretization methods such as those used in [13], [15]; at the price of additional approximation and increased computational requirements. In many cases, it may be preferable to maintain the simplicity of the MLM, while having a clear estimation about inaccuracies owing to violating modeling limits (e.g., non 1-D and non-sinusoidal effects), and thus avoid the computationally-demanding and non-intuitive discretization process, and keep the complexity manageable for analytical analysis. It was shown in [1] that the MLM can provide reasonable accuracy in predicting the port impedances without extensive modeling of non 1-D effects in single-frequency planar magnetics designs with sinusoidal waveforms. In this paper, we focus on evaluating the applicability and limitations of the proposed method in circuit simulations in the presence of substantial non 1-D and non-sinusoidal conditions, without using linearization or discretization.

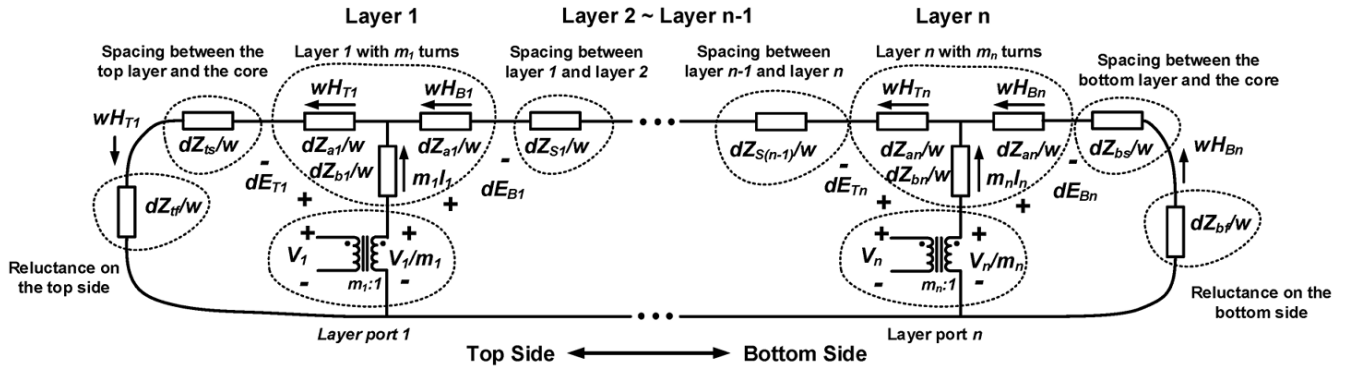


Fig. 2. Lumped circuit model consisting of many modular sub-circuits, each representing a portion of the physical planar magnetic structure.

The remainder of this paper is organized as follows: section II provides a brief overview of the MLM modeling approach and the *M2Spice* software tool. The frequency dependent behavior of the MLM approach is analyzed in section III. Section IV-A investigates the applicability and limitations of the MLM time-domain simulation approach with a single-frequency experimental setup that has substantial non-1D effects (e.g. fringing effects, edge effects). In section IV-B, the investigation is further extended to a practical magnetics design that is simulated and tested together with a dc-dc converter. Section V summarizes the applicability and limitations of the proposed “planar-magnetics-in-the-circuit” simulation approach. Finally, section VI concludes the paper.

II. MLM AND *M2Spice* OVERVIEW

Here we briefly introduce the modular layer model (MLM) presented in [1]. A multilayer planar magnetic structure as shown in Fig. 1a can be modeled as a combination of multiple circuit blocks as shown in Fig. 1b, and represented by a lumped circuit model comprising many iterative sub-circuit blocks as shown in Fig. 2. Each sub-circuit block represents a portion of the magnetic structure, including the magnetic reluctance on top of the layer stack, the conductor layers, the spacings, and the magnetic reluctance below the layer stack. This model can analytically capture skin- and proximity-effects in the windings under 1-D and MQS assumptions [1]. The cross and through variables in the lumped circuit model, i.e., values of E and H in Fig. 2, represent the current density and the field strength in the magnetic structure. By simulating this lumped circuit model with the external driving circuits and probing the current flowing through the corresponding sub-circuit in the SPICE simulation, the current flowing through each layer can be visualized and evaluated in SPICE.

A software tool – *M2Spice* – that can rapidly compute the element values, and automatically generate a SPICE netlist has been created to minimize the additional effort of using the model. Figure 3 shows its user interface. This tool is open-sourced by the authors¹ and is utilized for the studies here. Fig. 4 shows the information flow in the *M2Spice*-assisted design approach. The magnetic geometry information is first processed by *M2Spice*, which produces a netlist

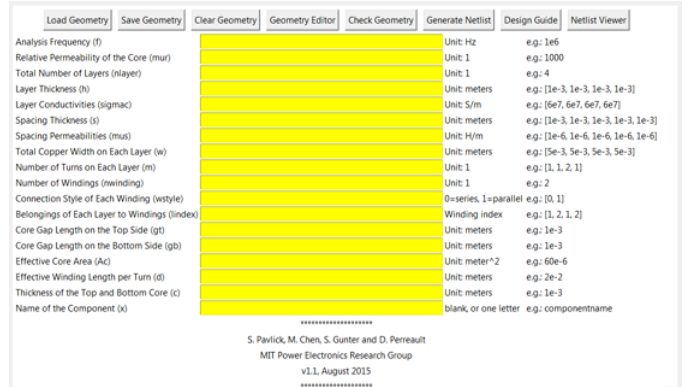


Fig. 3. Screenshot of the user-interface of the *M2Spice* tool.

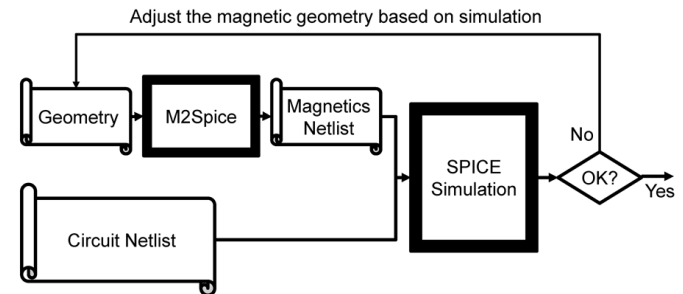


Fig. 4. Information flow of the *M2Spice*-based magnetics design approach.

for a subcircuit that captures the electrical behavior of the magnetic component. This netlist is combined with a netlist that represents other elements in the circuit (e.g., capacitors, resistors, switching devices, etc.) and fed into a SPICE simulation platform (e.g., *LTSpice*). Based on the simulated circuit performance, designers can very quickly adjust the geometry of the magnetic component (e.g., layer thickness, interleaving patterns, core shapes, etc.), and iterate the design.

III. FREQUENCY DEPENDENT IMPEDANCE VALUES

This section analyzes the applicability and limitations of using the MLM in circuit simulations. Assuming the permeability and permittivity of all materials stay constant across the full operating range, many elements in the MLM are

¹*M2Spice* [Online]. Available: <http://www.rle.mit.edu/per/M2Spice/>.

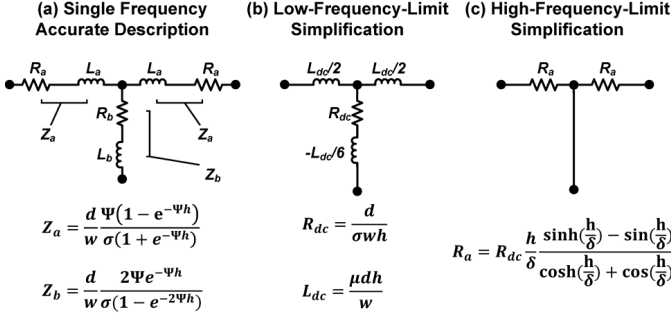


Fig. 5. (a) Single frequency T network of the MLM and (b) its Low-Frequency-Limit (LFL) simplification (i.e., when $h \ll \delta$), and (c) its High-Frequency-Limit (HFL) simplification (i.e., when $h \gg \delta$).

frequency independent, e.g. those representing the spacing and the magnetic core (Z_{tf} , Z_{ts} , $Z_{S1} - Z_{S(n-1)}$, Z_{bs} , and Z_{bf} in Fig. 2), as well as the wire connections describing how each layer is connected to other layers. There is generally no limitation in using these element values in SPICE simulations.

Elements related to the conductor layers are frequency dependent. As derived in [1] and shown in Fig. 5, the accurate netlist representing each conductor layer consists of two impedances, Z_a , and Z_b . They can be calculated using:

$$\begin{cases} Z_a = \frac{d\Psi(1 - e^{-\Psi h})}{w\sigma(1 + e^{-\Psi h})} \\ Z_b = \frac{2d\Psi e^{-\Psi h}}{w\sigma(1 - e^{-2\Psi h})} \end{cases} \quad (1)$$

where d is the conductor length per turn, w is the total width of the copper on this layer, h is the thickness, $\Psi = \frac{1+j}{\delta}$, where $\delta = \sqrt{\frac{2}{\omega\mu\sigma}}$ is the skin depth of the conductor, μ is its permeability, σ is the conductivity, and ω is the angular frequency. In the netlist generated by *M2Spice*, each complex impedance is represented by a resistor and an inductor, which can have positive or negative values, i.e., $Z_a = R_a + \omega L_a j$, and $Z_b = R_b + \omega L_b j$, as shown in Fig. 5a.

Since Z_a and Z_b are both frequency dependent, R_a , R_b , L_a , and L_b are all frequency dependent. As derived in Appendix I, when $\omega \rightarrow 0$, R_a approaches zero; L_a has a limit of $\frac{\mu d h}{w}$; R_b has a limit of $\frac{d}{\sigma w h}$; and L_b has a limit of $-\frac{\mu d h}{6w}$. We name these element values as Low-Frequency-Limit (LFL) element values. And when $\omega \rightarrow +\infty$, R_b , L_a , and L_b all approach zero, and $R_a = \frac{d}{\sigma w \delta} \frac{\sinh(h/\delta) - \sin(h/\delta)}{\cosh(h/\delta) + \cos(h/\delta)}$. We name these element values as High-Frequency-Limit (HFL) element values.²

R_a , L_a , R_b , and L_b are normalized to their LFL values to investigate their frequency dependent characteristics. We define the dc resistance of a copper layer with thickness h , width w , and length d , as R_{dc} equals $\frac{d}{w\sigma h}$; and the inductance of a spacing with thickness h , width w , and length d , as L_{dc} equals $\frac{\mu d h}{w}$. Defining $\Delta = h/\delta$, then

²The LFL and HFL values can be utilized in further simplified MLM modeling (but still capture a major amount of information, especially the loss) as illustrated in Fig. 6: if $h \gg \delta$ for the frequency range of interest, HFL element values should be used; if $h \ll \delta$, LFL element values should be used. Intuitively, at low frequencies, the inductive behavior and the dc resistance dominates the conductor behavior; and at high frequencies, the reactive energy stored in the conductor diminishes, leaving only the ac resistance dominating the conductor behavior.

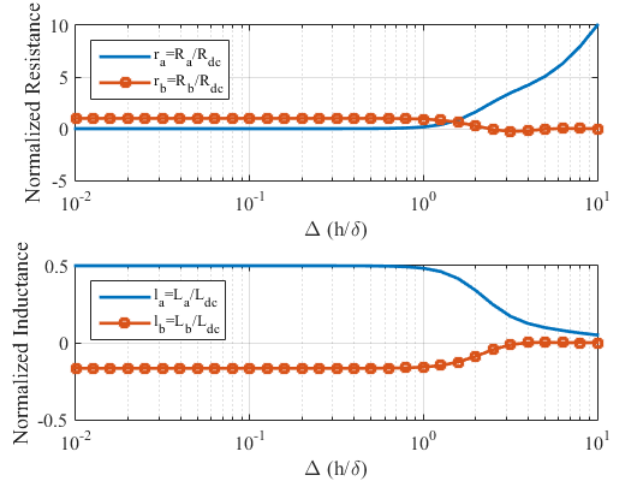


Fig. 6. Normalized impedance values of the elements in the T network of Fig. 5a as functions of Δ .

$$\begin{cases} r_a = \frac{R_a}{R_{dc}} = \Re e \left(\frac{(1+j)\Delta(1 - e^{-(1+j)\Delta})}{1 + e^{-(1+j)\Delta}} \right) \\ l_a = \frac{L_a}{L_{dc}} = \Im m \left(\frac{j(1 - e^{-(1+j)\Delta})}{(1+j)\Delta(1 + e^{-(1+j)\Delta})} \right) \\ r_b = \frac{R_b}{R_{dc}} = \Re e \left(\frac{2(1+j)\Delta e^{-(1+j)\Delta}}{1 - e^{-2(1+j)\Delta}} \right) \\ l_b = \frac{L_b}{L_{dc}} = \Im m \left(\frac{2je^{-(1+j)\Delta}}{(1+j)\Delta(1 - e^{-2(1+j)\Delta})} \right) \end{cases} \quad (2)$$

$\Re e$ represents the real part of a complex value, and $\Im m$ represents the imaginary part of a complex value. r_a , l_a , r_b , and l_b are plotted as functions of Δ in Fig. 6. Note $\Delta = 1$ indicates the frequency at which the layer thickness equals the skin depth ($h=\delta$).

Figure 6 indicates that for non-sinusoidal waveforms with harmonics distributed in multiple frequencies, if a majority of its harmonic components are in the low frequency ($\Delta < 1$) range (including dc), using the netlist generated at the fundamental frequency of this circuit is accurate, because the element values stay relatively constant across the whole frequency range. If a majority of its harmonic components are distributed at multiple frequencies in the high frequency ($\Delta > 3$) range, then a single frequency netlist cannot capture the wide-band behaviors of the magnetic components. As discussed in Appendix II, under this situation, concepts of effective frequency [21] can be utilized, which offers conservation of loss according to Fourier Analysis.

IV. EXPERIMENTAL VERIFICATION

It is clear that the MLM approach – with layer stacking and frequency dependent impedances included – can always provide more information than many conventional magnetic models. An interesting question is how accurate an MLM-based time-domain simulation is in predicting the current distribution and loss in the magnetics (when the magnetics are simulated together with the circuit). To answer this question, we investigate the applicability and limitations of the MLM-based time-domain simulation method by comparing the SPICE simulation results with experimental measurements

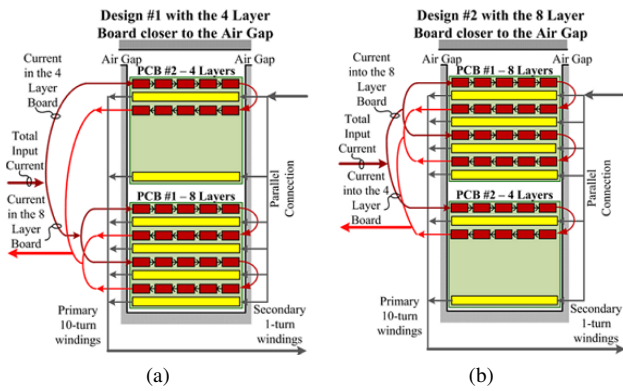


Fig. 7. Cross-section view of the layer stack of the two coupled inductors (a) Design #1 and (b) Design #2. Note that the dimension of this stackup is not to scale.

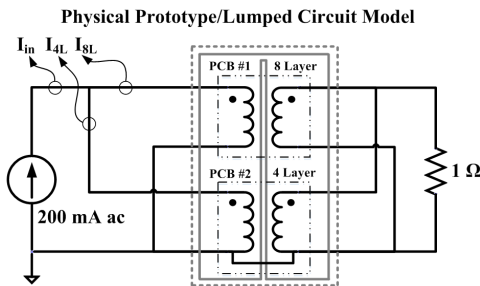


Fig. 8. Circuit structure of the test setup. The leakage and magnetizing inductances are included in the dashed circuit block.

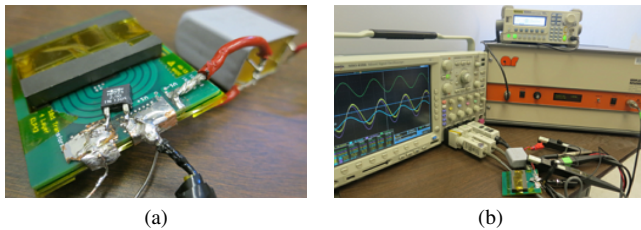


Fig. 9. (a) Photo of the prototype. (b) Experimental setup.

in two setups. The first setup investigates a coupled inductor design with sophisticated winding patterns, but only with a single frequency component. The second setup is the design of multiple magnetic components in a newly presented circuit architecture that has switching harmonics [22].

A. Design Evaluation in a Purely Sinusoidal Setup

In this setup, the simulation and experimental waveforms of two 10:1 coupled inductors with identical cores but different layer stack-ups are compared. Figure 7 shows the cross-section view of the two coupled inductors. The winding structure of the two coupled inductors are manufactured with two 72 mil printed-circuit boards (PCB #1 and #2), which are linked by a single EPCOS ELP43 core (N49 material) with a distributed air gap on top of both the center and side legs. PCB #1 has eight copper layers and PCB #2 has four copper layers. All layers are 4 oz copper layers. In Design #1, the 4-layer board is placed on top of the 8-layer board, and is closer to the air gap (Fig. 7a); in Design #2, the 8-layer board is placed on top of the 4-layer board, and is closer to the air gap (Fig. 7b). The

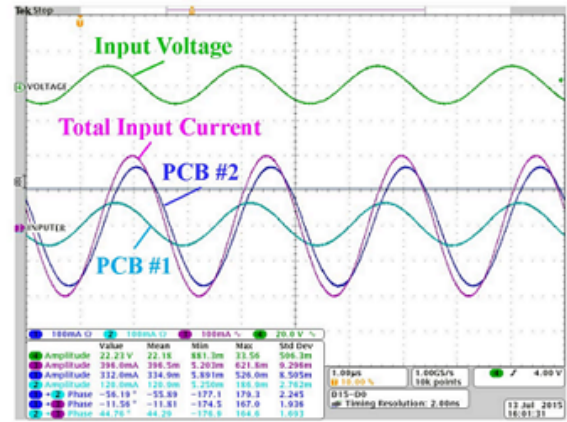


Fig. 10. Measured waveforms for Design #1 at 400 kHz.

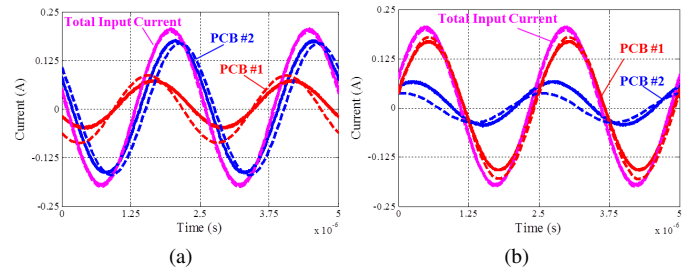
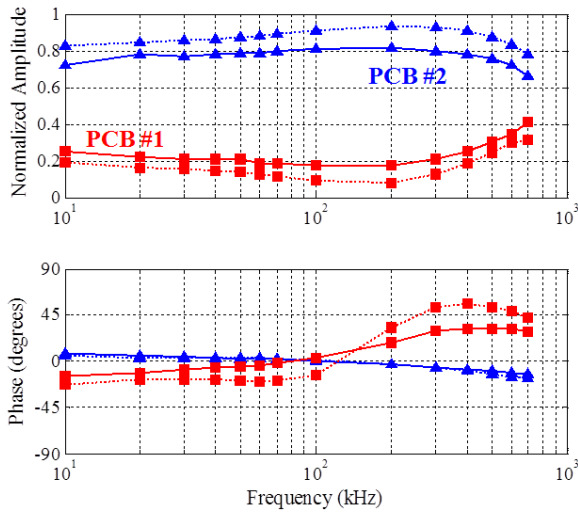


Fig. 11. Simulation and experimental waveforms showing the current sharing between the two primary windings at 400 kHz. (a) Design #1: PCB #2 (4 layer) on top. (b) Design #2: PCB #1 (8 layer) on top. Solid line: experimental waveform. Dashed line: simulated waveform.

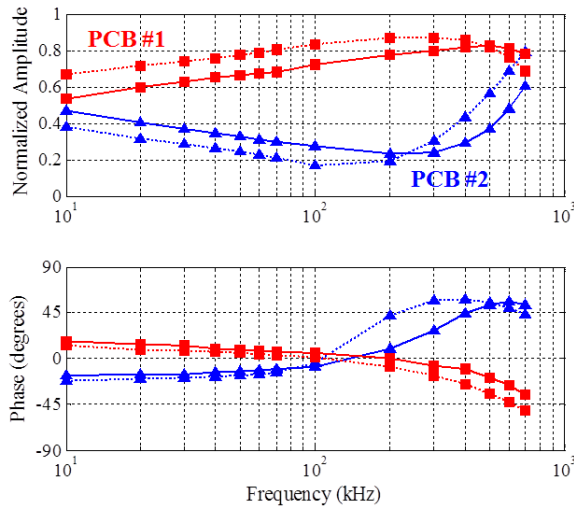
odd layers (from the top) of both PCBs each have five spiral series-connected turns. Layers 1&3 and 5&7 of PCB #1, and layers 1&3 of PCB #2 are each connected into a series-tied pair to formulate three 10-turn windings (red layers of Fig. 7). These three 10-turn windings are then connected in parallel as primary windings. The even layers of both PCBs each have a single turn and are connected in parallel to form a six layer 1-turn secondary winding (yellow layers of Fig. 7).

Figure 8 shows the schematic of the test circuit. A film capacitor (not shown) is connected in series with the input source to block the dc component. The current in the 4-layer PCB, in the 8-layer PCB and the total input current (I_{AL} , I_{8L} and I_{in}) are observed using TCP202 and TCP0030 current probes. Since the two PCBs are stacked and are linked with a single core, they ideally have identical flux linkage and identical voltage-drop per turn. The different ac impedance of the two boards will create unbalanced current sharing between their copper layers. Intuitively, at direct current (dc) or low frequency alternate current (ac), the 8-layer board has a lower resistance and will always carry more current. However, high frequency ac current will tend to flow in the board that is closer to the gap, redistributing the current and creating interesting phenomena that we seek to visualize in time-domain simulations.

Figure 9a shows the prototype planar coupled inductor with the blocking capacitor and terminating resistor. Fig. 9b shows the experimental bench setup. The gain of the power amplifier



(a)



(b)

Fig. 12. Comparison of the amplitude and phase of the currents for the experimental (solid lines) and simulated results (dashed lines). (a) Design #1: PCB #2 (4 layer) on top. (b) Design #2: PCB #1 (8 layer) on top. The amplitude and phase of each PCB is normalized to the input current (200 mA). The phase is positive if the PCB current leads the input current.

is tuned to make the total input current 200 mA (peak). The 1 ohm load resistor has a constant resistance across the full frequency range.

Using the MLM-based approach, the geometry of the magnetic circuit including the two planar winding structures is processed by *M2Spice* to generate the SPICE netlist. The cross winding capacitance is modeled separately with EQS methods [6]. The layer-to-layer capacitance of the prototype lumped to the secondary is calculated to be 150 nF. The netlist is then imported into *LTSpice* and simulated. The three currents are then modeled using time-domain simulations. In *LTSpice*, the device is constantly driven by a 200 mA ac current source and the frequency is swept from 10 kHz to 700 kHz (with a netlist generated for each frequency). We intentionally isolated the modeling and the measurement process, i.e., all modeling efforts are rigorously developed based on a priori design information (the known system geometry only), without

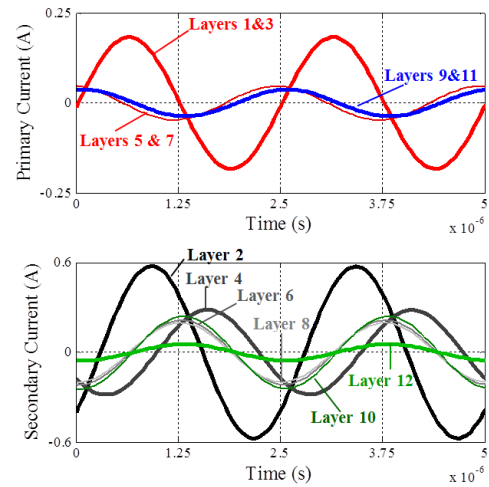


Fig. 13. Simulated current distribution in all 12 layers of Design #1 at 400 kHz using time-domain *LTSpice* simulations based on the *M2Spice* subcircuit. The layers are numbered from top to bottom with layer 1 closest to the gap. Each primary winding consists of two layers.

information gathered after the prototype was built.

Figure 10 shows the measured waveforms of Design #1 at 400 kHz. Figure 11 compares the simulated and measured current waveforms of the two layer stacks operating at 400 kHz. The simulated waveforms match well with the experimental waveforms. The time-domain SPICE simulation based on the MLM as generated by *M2Spice* can accurately predict the current distribution between two parallel windings at different frequencies. The time-domain simulation is capable of accurately quantifying the phenomenon that the PCB closer to the air gap carries more current regardless of its dc resistance.

Figure 12 compares the simulated and measured amplitudes and phases of the current flowing through the two layer stacks across a frequency range of 10 kHz–700 kHz (with netlists separately generated for each frequency). As frequency increases, it can be seen that the phase shift between the two PCB currents also increases, especially when the frequency is above 100 kHz. As a result of the increased phase shift, the amplitude increases in the bottom PCB, indicating circulating currents and higher overall rms current.

The experimental measurement can only reveal the current sharing between the two PCBs (grouping multiple layers). An experimental effort to determine the current distribution in all 12 layers is extremely challenging, because any additional current measurement infrastructure needs to be accurately modeled and calibrated, and will involve new approximations. While hard to do experimentally, the current distribution in the 12 layers can be easily visualized using SPICE time-domain simulations. Fig. 13 shows the current distribution in the 12 layers in Design #1 of Fig. 7a. As expected, the series-connected pairs have identical current distribution (layers 1&3, layers 5&7 and layers 9&11), and the parallel layers unevenly share the current with dramatic phase shift.

To validate the current distribution shown in simulation, we predict the current distribution using Ansoft Maxwell 2D simulations. To emulate the condition that the magnetic component is connected to the circuit, the external drive

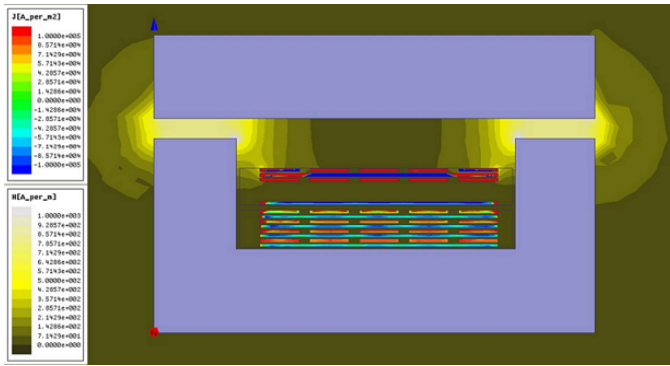


Fig. 14. FEM simulation results for an instantaneous current and field distribution of Design #1 with the 4-layer board on top when the total primary side current is 200 mA at 0 degrees.

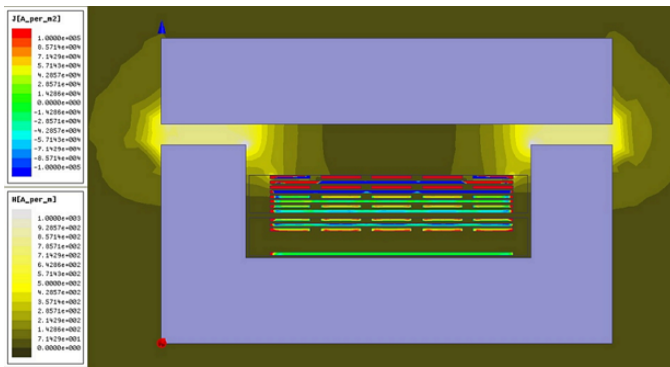


Fig. 15. FEM simulation results for an instantaneous current and field distribution of Design #2 with the 8-layer board on top when the total primary side current is 200 mA at 0 degrees.

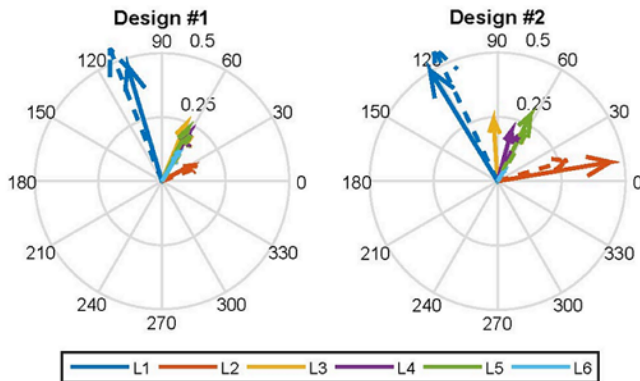


Fig. 16. Polar plot of the SPICE and FEM predicted current sharing in all 6 paralleled secondary layers in Design #1 and Design #2 when the total primary side current is 200 mA at 0 degrees. Solid arrows: FEM results; Dashed arrows: SPICE results. Different colors indicate different layers: L1–top secondary layer; L6–bottom secondary layer.

current for the magnetic component is pre-determined by SPICE simulation, and the current distribution inside the layers is solved by FEM. The FEM-simulated current and field distribution in Design #1 and Design #2 are shown in Fig. 14–15, and the SPICE predicted and FEM predicted amplitude and phase of the current in all 6 secondary layers are compared in Fig. 16. The current distribution predicted by *M2Spice*

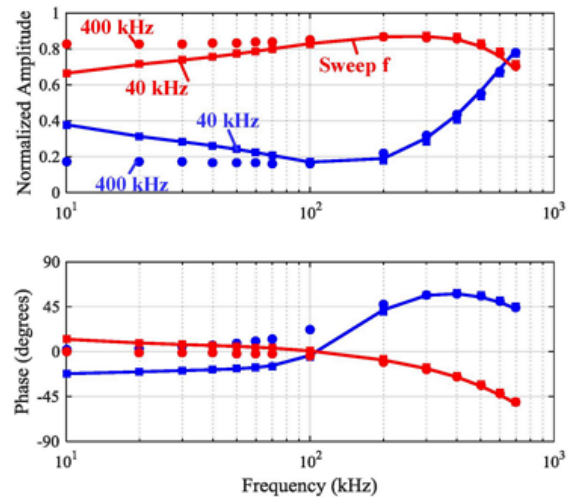


Fig. 17. Comparing the simulation results of Design #2 using single-frequency netlists (square: 40 kHz, or circle: 400 kHz) to visualize the current distribution across a wide frequency range (10 kHz–700 kHz), and the results of using different netlists for different frequencies (solid curve: Sweep f).

TABLE I
SPICE SIMULATION AND FEM PREDICTED TOTAL LOSS AT 400 KHz.

Total Loss in All Layers # (mW)	SPICE	FEM
Design #1, 12 layers in total, 4 layer top, 8 layer bottom	10.511	7.997
Design #2, 12 layers in total, 8 layer top, 4 layer bottom	10.511	8.007
Design #3, 8 layers in total, with the 8 layer PCB	9.759	4.287
Design #4, 4 layers in total, with the 4 layer PCB	10.122	4.667

matches well with that predicted by the FEM tool, even with the presence of substantial 2-D effects (including both fringing fields and vertical spacings among primary layers).

To investigate the limitation of the model in predicting wide-band behaviors, two single-frequency netlists (40 kHz and 400 kHz) are used to simulate the current distribution across a wide frequency range (10 kHz–700 kHz). Fig. 17 compares the simulated results with simulations that use different netlists for different frequencies (solid line, labeled as “Sweep f”). The netlist generated for 40 kHz can well model the current distribution across a wide frequency range up to the frequency when $\Delta = 1$ (for 4 oz copper, this frequency is 226 kHz), while the netlist generated for 400 kHz operation only shows a close match only if the frequency is in the hundreds of kHz. This limitation matches the analysis presented in Section III.

Unfortunately, a well matched turn-level current distribution does not guarantee good prediction of loss. 2-D factors change the current density along the width of the conductor – an effect which is not captured by the 1-D method. Moreover, estimating the loss in the time domain naturally involves integration, which brings in quantization noise in SPICE simulations. We compared the loss of Design #1 and Design #2 when they are simulated in SPICE³ and FEM⁴ under the setup

³LTS Spice v4.23h – Solver=alternate, Tctrl=1, Max thread=2.

⁴Ansoft Maxwell 2D v16.0 – EddyCurrent Simulation

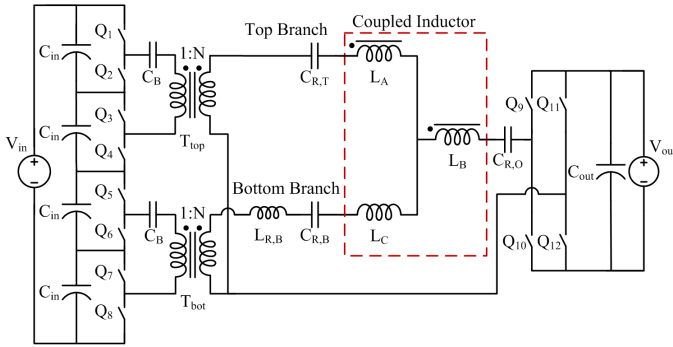


Fig. 18. Proposed implementation of the ICN converter [22]. The ICN incorporates harmonic filtering through the use of resonant tanks as well as two equal but opposite impedances. This structure contains four magnetic structures - two transformers, a coupled inductor (indicated by the red-dashed box), and a resonant inductor.

of Fig. 8. We also took the 4 layer PCB away from Design #1 and the 8 layer PCB away from Design #2 to investigate the impacts of fringing fields to the total loss. Table I lists the predicted losses. Although the loss values are slightly mismatched in magnitude, SPICE simulation does indicate an interesting trend that designs with less copper layers may actually perform better in terms of loss in certain setups (even without considering the fringing effects). This is correct though it is contradictory to the common misconception that adding more copper layers usually helps to reduce the loss. The trend can be likely be explained by proximity effect and the resultant phase shifting of the layer currents.

B. Design Evaluation in a Switched-Mode-Power-Converter

This section investigates the applicability and limitations of an MLM-based simulation approach in a recently published power converter containing sophisticated planar magnetic structures - the Impedance Control Network (ICN) resonant converter [22] as shown in Fig. 18. It has two transformers, a resonant inductor, and a coupled inductor. This converter is designed to operate with an input voltage of 260 V–410 V, an output voltage of 12 V, and a rated output power of 300 W. The operating frequency is set to 500 kHz. Detailed operation of the ICN converter is presented in [22]. Using this converter as a test platform, we tried to visualize the current distribution in the magnetic components using *M2Spice*, and investigate the applicability of the MLM approach for predicting the loss of the magnetics when it is simulated with the full converter.

We first investigate the capability of SPICE simulation in predicting current distribution. The ICN converter has two transformers. The winding of each transformer was built using two copies of PCB #1 used in section IV, which are coupled with a single ELP43 core with N49 material (the two PCBs are paralleled in the same manner as described in Fig. 8 but now both PCBs are the 8 layer version). The PCBs both have 4 oz copper layer thickness (the frequency when h equals Δ is 226 kHz). Here we focus on the current sharing in the two PCBs under two operating modes - 260 V and 410 V as shown in Figs. 19–20. A close match was found between measured and simulated results. When the input voltage is 260 V, the

TABLE II
SPICE SIMULATION PREDICTED LOSS FOR VARIOUS TRANSFORMER INTERLEAVING PATTERNS. P: PRIMARY LAYERS WITH 5 SERIES CONNECTED TURNS; S; SECONDARY LAYERS WITH 1 SINGLE TURN. "PSPS" REPRESENTS A FOUR LAYER INTERLEAVING PATTERN: THE 1st AND 3rd LAYERS ARE TWO PRIMARY LAYERS WITH 5 TURNS, THE 2nd AND 4th LAYERS ARE TWO SECONDARY LAYERS WITH 1 TURN.

Layer Stack	SPICE Predicted Loss
SSPP	3.8068 W
PPSS	3.7261 W
SPPS	2.9148 W
PSSP	2.8963 W
SPSP	2.8678 W
PSPS	2.8465 W
SSPPSSPP	2.2267 W
PPSSPPSS	2.1986 W
PSSPPSSP	2.0331 W
SPPSSPPS	2.0291 W
SPSPSPSP	1.9593 W
PSPSPSPS	1.9548 W
PSPSPSPSPSPSPSPS	1.9733 W
SPSPSPSPSPSPSPSP	1.9565 W

total input current was quite sinusoidal and well shared in the two boards (similar amplitude and phase). When the input voltage is 410 V, the current is more trapezoidal and there is a phase shift between the current injected into the top PCB and that in the bottom PCB, indicating circulating current, and additional loss. Other time-domain details, such as the soft-switching transition, and the high-order harmonics and their patterns, all matched well. As mentioned before, unlike in the experimental setup, it is easy to see the current distribution in all of the layers using *M2Spice* as shown in Fig. 21. By looking at the current in all of the primary layers, it can be seen that the phase shift between the two PCBs is a result of uneven current sharing in the topmost primary winding as opposed to all remaining windings. This winding is closest to the gap and therefore is the most different. It is verified in this example that in a practical design with sophisticated winding patterns and non-sinusoidal circuit driving patterns, the netlist generated by *M2Spice* can accurately predict the current distribution in planar magnetics in time domain simulations.

A further investigation is to use SPICE simulation in predicting the loss in magnetics, while the magnetic component is driven by the actual circuit. By measuring the current and voltage waveforms in SPICE, one is able to predict the loss in the magnetic components, and thus make appropriate design choices based on the loss information. For example, we used SPICE simulations to determine the most cost-effective number of fully interleaved primary-secondary pair sets in the transformers of Fig. 18. The losses predicted by SPICE for different design variations are listed in Table II. Increasing the layer count from 4 to 8 gives us substantial reduction in predicted loss (>40%). However, negligible improvements were found when the layer count increased beyond 8, which was verified in the experimental setup that was used to generate Figs. 19–20. This is the reason why the transformer

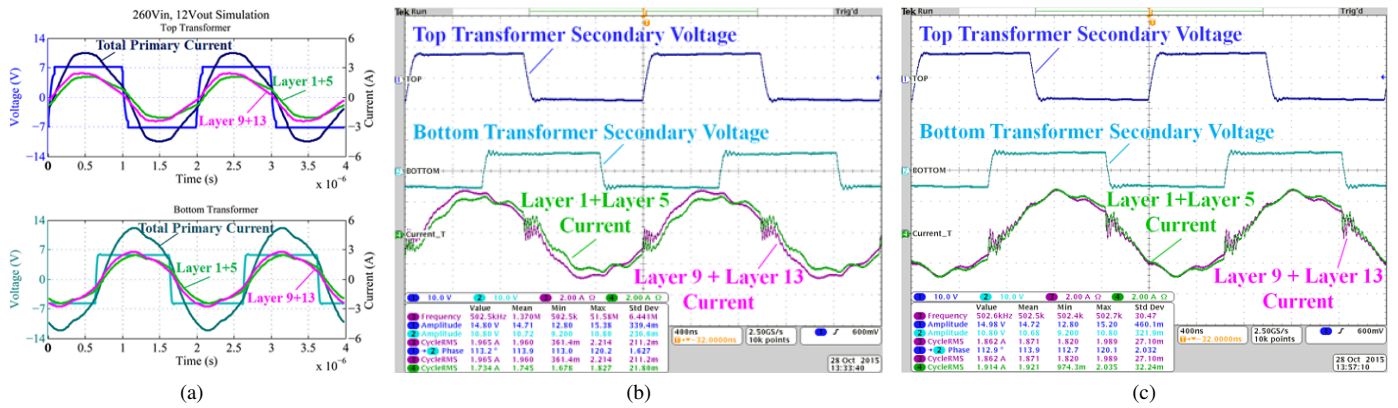


Fig. 19. (a) Simulated and (b)-(c) measured current sharing of the two PCBs in the ICN converter when the input voltage of the converter is 260 V. The current for the top transformer is shown in (b) and the current for the bottom transformer is shown in (c).

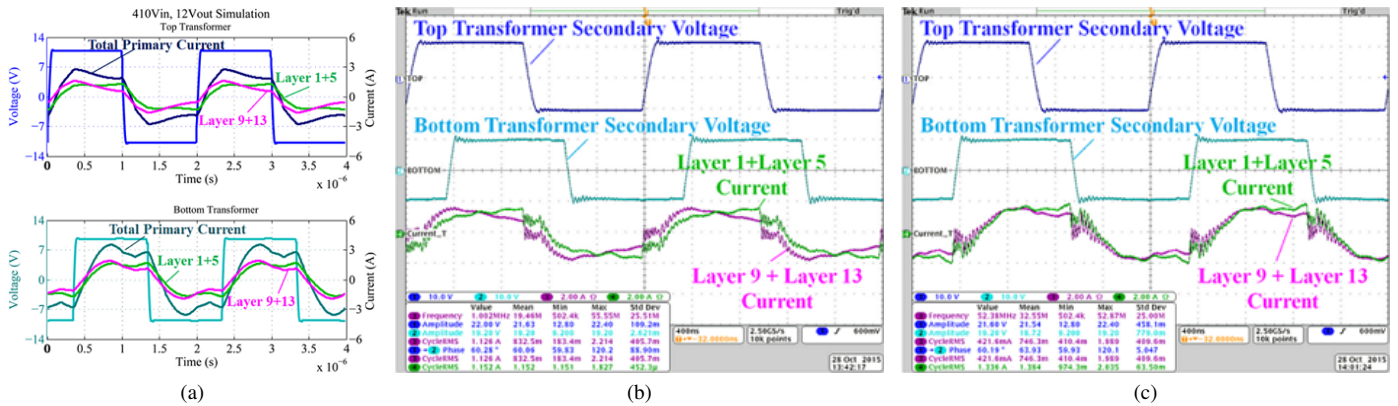


Fig. 20. (a) Simulated and (b)-(c) measured current sharing of the two PCBs in the ICN converter when the input voltage of the converter is 410 V. The current for the top transformer is shown in (b) and the current for the bottom transformer is shown in (c).

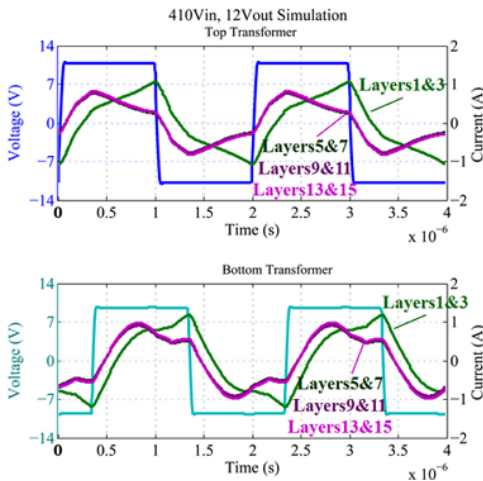


Fig. 21. Simulated current distribution in all 8 primary layers of the transformers at an input voltage of 410 V using the *M2Spice*-derived magnetics model. Significant harmonic waveform components are present. The layers are numbered from top to bottom with layer 1 closest to the gap. Each primary winding consists of two layers.

layer count was chosen as 8 in [22].

In the ICN converter, the two windings in the coupled inductor are effectively driven by two current sources. The amplitude and phase of each current source are highly dependent

on the circuit behavior. It is difficult to model the circuit and the coupled inductor separately as in conventional magnetics modeling approaches, or FEM. *M2Spice* allows the magnetic component to be evaluated together with the circuit in SPICE simulations. In the test setup, this inductor is implemented with the Coilcraft Planar Transformer Prototyping Kit [23]. The core is a PL140 core, and the primary and secondary windings⁵ are implemented with single-turn stamps. Each winding is created by multiple parallel stamps. To avoid the impact of temperature rise in experiments, the converter is operated in a low-power mode with 100 V input voltage, 5 V output voltage, and 10 A output current, and the total loss of the converter with different coupled inductor implementations is measured. The predicted and measured losses in multiple experimental setups are shown and compared in Table III. It can be seen that SPICE simulations do predict the trend that using parallel layers reduces the loss, having the secondary layer closer to the gap reduces the loss, and a more efficient coupled inductor design can help to reduce the total converter loss. At the same time, the quantitative predictions of total converter loss are not very accurate, in part because the SPICE model does not include many practical details (e.g., PCB trace losses, etc.) which are important in this design example.

⁵The primary (P) winding is denoted as the single turn forming L_A in Fig. 18 and the secondary (S) winding is denoted as the single turn forming L_B in Fig. 18.

TABLE III

SPICE SIMULATION PREDICTED LOSS IN THE COUPLED INDUCTOR AND TOTAL SYSTEM, EXPERIMENTAL MEASURED LOSS IN THE TOTAL SYSTEM.

Interleaving	SPICE		Experimental
	Inductor Loss	Total Converter Loss	Total Converter Loss
PS	0.91973 W	4.749 W	14.008 W
SP	0.89358 W	4.638 W	12.721 W
PSPS	0.72098 W	4.455 W	11.047 W
SPSP	0.61108 W	4.382 W	10.627 W

V. SUMMARY OF THE APPLICABILITY AND LIMITATIONS

Applicability:

- 1) *M2Spice*-assisted circuit simulations can usually provide more information than conventional magnetic models.
- 2) *M2Spice*-assisted circuit simulations allow magnetic components to be analyzed together with external drive circuits – a function that conventional magnetics modeling approaches and commercial FEM tools⁶ do not offer.
- 3) *M2Spice*-assisted circuit simulations are highly applicable in visualizing the current distribution in planar magnetics even with substantial non-1D or non-sinusoidal factors in switched-mode-power-converters. It can also usually provide useful qualitative loss comparison information in a rapid design iteration process.

Limitations:

- 1) *M2Spice*-assisted circuit simulations may not be able to accurately predict the current distribution if the circuit has wide-frequency-range harmonic components.
- 2) *M2Spice*-assisted circuit simulations cannot always accurately predict the absolute loss in magnetic components having very broadband excitation, for a number of reasons, but including violations of the 1-D constraints under which the model is developed.

VI. CONCLUSIONS

“Magnetics-in-the-circuit” time-domain SPICE simulations can facilitate quick circuit design iterations. This paper introduced a software tool *-M2Spice* – and investigates its applicability and limitations in evaluating various planar magnetics designs with “planar-magnetics-in-the-circuit” time domain simulations. It is verified that time-domain SPICE simulations with *M2Spice*-generated netlists can accurately predict current sharing in multiple layers and parallel layers, even if significant non-1D effects are present. If there is one fundamental frequency component dominating, simulating the circuit with a netlist generated at a single frequency can offer substantial efficiency in visualizing the current distribution. SPICE simulation cannot accurately predict loss if there are significant non-1D effects and/or broadband excitation waveforms, but can illustrate the loss trend for different interleaving patterns, and thus can assist evaluation of different planar magnetics implementations.

⁶Some FEM tools offer “magnetic-in-circuit” joint-design functions, but the design options are usually limited to a few commonly-used topologies.

ACKNOWLEDGEMENTS

The authors gratefully acknowledge C. R. Sullivan of Dartmouth College for the helpful discussion, and the support provided for this work by Texas Instruments and by the National Science Foundation under NSF award number 1307699.

APPENDIX I: DC LIMITS OF THE ELEMENTS IN THE T NETWORK

When $\omega \rightarrow 0$, $\delta \rightarrow \infty$, and $\Psi \rightarrow 0$. The first-order Taylor series expansion of $e^{-\Psi h}$ around $\Psi = 0$ is $1 - \Psi h$. Using this approximation, the limit of Z_a as $\Psi \rightarrow 0$ is

$$\lim_{\Psi \rightarrow 0} Z_a = \frac{\mu d h}{2w} \omega j \quad (3)$$

Therefore, Z_a can be approximated as an inductor with its inductance equal to $L_{a,dc} = \frac{\mu d h}{2w}$. The dc resistance of this branch is zero ($R_{a,dc} = 0$). As an intuitive verification, assuming there is no current in the conductor, the inductance of a spacing that has a thickness of h is $L_s = \frac{\mu d h}{w}$. $L_{a,dc}$ is effectively one half of L_s .

Taking the third-order Taylor series expansion of $e^{-\Psi h}$ and $e^{\Psi h}$ around $\Psi = 0$ will yield:

$$Z_b \approx \frac{d(1 - j \frac{h^2 \omega \mu \sigma}{6})}{w \sigma h (1 + \frac{(h^2 \omega \mu \sigma)^2}{36})} \quad (4)$$

$$\lim_{\omega \rightarrow 0} Z_b = \frac{d}{w \sigma h} - \frac{\mu d h}{6w} \omega j \quad (5)$$

Thus, when $\omega \rightarrow 0$, Z_b can be approximated as a resistance of $R_{b,dc} = \frac{d}{w \sigma h}$ in series with an inductance of $L_{b,dc} = -\frac{\mu d h}{6w}$.

APPENDIX II: NON-SINUSOIDAL WAVEFORMS AND EFFECTIVE FREQUENCY

For systems with a single frequency (e.g. resonant converters with sinusoidal waveforms), a single frequency netlist is well-suited to time-domain simulations. For non-sinusoidal waveforms with harmonics, we still propose to use a single frequency netlist for time-domain simulations to retain the simplicity and convenience of the MLM method. As shown in Fig. 6, when $\Delta < 1$, r_a , r_b , l_a and l_b stay relatively constant across wide frequency range, and can be directly used for wide spectrum simulation. When $\Delta > 1$, r_b , l_a and l_b all rapidly approach zero. As a result, the key frequency dependent element is r_a , which can be rewritten as:

$$r_a = \Delta \frac{\sinh \Delta - \sin \Delta}{\cosh \Delta + \cos \Delta}. \quad (6)$$

The value of r_a is plot in Fig. 22 in log scale. When $\Delta < 2$, r_a is proportional to Δ^4 , indicating that the resistance is proportional to f^2 (proximity effects are more significant than skin effects). When $\Delta > 3$, r_a is proportional to Δ , indicating that the resistance is proportional to \sqrt{f} (skin effects are more significant than proximity effects).

Non-sinusoidal current waveforms (waveforms having one or more significant harmonics) can be treated by Fourier analysis utilizing the effective frequency concept described by Eq. 26 in [21]. This way of choosing the effective frequency

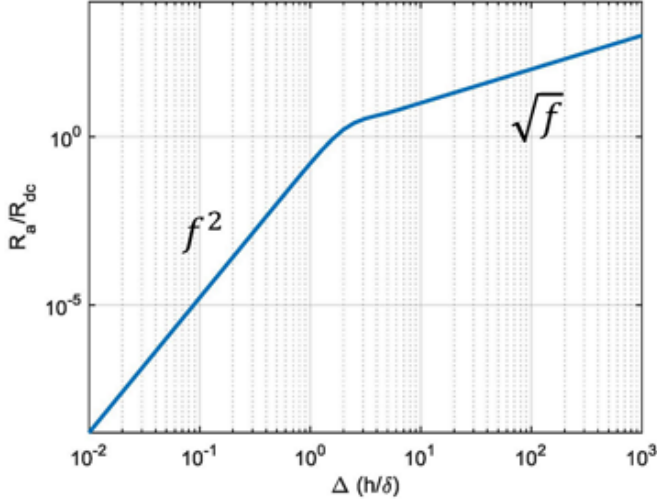


Fig. 22. Normalized R_a value in the T network as a function of Δ . R_a is the most frequency sensitive element in the network, and can be used to select the effective frequency. When $\Delta < 1$, R_a is proportional to f^2 (Δ^4). When $\Delta > 1$, R_a is proportional to \sqrt{f} (Δ).

is derived based on a conservation of the loss, which is the major optimization goal for many designs. In the MLM model, r_a and r_b are loss contributing components. For a waveform shape with a majority of its harmonic components distributed in the low frequency ($\Delta < 1$) range (this case includes waveforms comprising significant dc components), since r_a is proportional to f^2 and r_b , l_a , and l_b stay constant, the effective frequency, F_{eff} , that can be used to generate the single-frequency netlist can be selected as:

$$F_{eff|\Delta < 1} = \sqrt{\frac{\sum_{j=0}^{\infty} I_j^2 f_j^2}{\sum_{j=0}^{\infty} I_j^2}} \quad (7)$$

I_j is the rms value of the respected harmonic component, and f_j is the respected harmonic frequency. Simplified methods of calculating F_{eff} , and the Fourier coefficients of many typical waveforms are provided in [7].

For a waveform shape with a majority of its harmonic components distributed in the high frequency range (i.e., $\Delta > 3$) range, r_a is proportional to \sqrt{f} , and r_b , l_a , l_b rapidly approach zero. As a result, the effective frequency used for generating the netlist can be selected as:

$$F_{eff|\Delta > 3} = \left(\frac{\sum_{j=0}^{\infty} I_j^2 \sqrt{f_j}}{\sum_{j=0}^{\infty} I_j^2} \right)^2 \quad (8)$$

For cases when harmonic components are not all located in either the $\Delta < 1$ or $\Delta > 3$ region, since r_b also changes across frequencies (drops from 1 to zero as Δ increases from 1 to 3) and may have significant impact, we do not suggest one single effective frequency for the time-domain simulation. Nevertheless, one can always simulate the magnetics at different frequencies (with netlists generated for different frequencies), and apply superposition to these single frequency results.

REFERENCES

- [1] M. Chen, M. Araghchini, K. K. Afridi, J. H. Lang, C. R. Sullivan, and D. J. Perreault, "A systematic approach to modeling impedances and current distribution in planar magnetics," *IEEE Trans. Power Electron.*, vol.31, no.1, pp. 560-580, January, 2016.
- [2] M. T. Quirke, J. J. Barrett, and M. Hayes, "Planar magnetic component technology-a review," *IEEE Trans. Compon. Hybrids, Manuf. Technol.*, vol.15, no.5, pp.884-892, Oct. 1992.
- [3] C. R. Sullivan, D. V. Harburg, J. Qiu, C.G. Levey, and D. Yao, "Integrating magnetics for on-chip power: a perspective," *IEEE Trans. Power Electron.*, vol.28, no.9, pp.4342-4353, September 2013.
- [4] Z. Ouyang and M. Andersen, "Overview of planar magnetic technology fundamental properties", *IEEE Trans. Power Electron.*, vol.29, no.9, September 2014.
- [5] P. L. Dowell, "Effects of eddy currents in transformer windings," *Proc. of the Institution of Electrical Engineers*, vol.113, no.8, pp.1387-1394, August 1966.
- [6] A. F. Goldberg, J. G. Kassakian, and M. F. Schlecht, "Issues related to 1-10-MHz transformer design," *IEEE Trans. Power Electron.*, vol.4, no.1, pp.113-123, January 1989.
- [7] W. G. Hurley, E. Gath, and J. G. Breslin, "Optimizing the AC resistance of multilayer transformer windings with arbitrary current waveforms," *IEEE Trans. Power Electron.*, vol.15, no.2, pp.369-376, Mar. 2000.
- [8] Y. Han, G. Cheung, A. Li, C. R. Sullivan, and D. J. Perreault, "Evaluation of magnetic materials for very high frequency power applications," *IEEE Trans. Power Electron.*, vol.27, no.1, pp.425-435, Jan. 2012.
- [9] J. A. Ferreira, "Improved analytical modeling of conductive losses in magnetic components," *IEEE Trans. Power Electron.*, vol.9, no.1, pp.127-131, Jan 1994.
- [10] R. W. Erickson and D. Maksimovic, "A multiple-winding magnetics model having directly measurable parameters," *Proc. of the IEEE Power Electron. Special. Conf. (PESC)*, vol.2, pp.1472-1478, 17-22, May 1998.
- [11] J.H. Spreen, "Electrical terminal representation of conductor loss in transformers," *IEEE Trans. Power Electron.*, vol.5, no.4, pp.424-429, Oct. 1990.
- [12] D. C., Hamill, "Lumped equivalent circuits of magnetic components: the gyrator-capacitor approach," *IEEE Trans. Power Electron.*, vol.8, no.2, pp.97-103, Apr 1993.
- [13] J.-P. Keradec, B. Cogitore, and F. Blache, "Power transfer in a two winding transformer: from 1-D propagation to an equivalent circuit," *IEEE Trans. Magn.*, vol.32, no.1, pp.274-280, Jan. 1996.
- [14] J. M. Lopera, M. Pernia, J. Diaz, J. M. Alonso, and F. Nuno, "A complete transformer electric model, including frequency and geometry effects," *Proc. of the IEEE Power Electron. Special. Conf. (PESC)*, vol.2, pp.1247-1252, June 1992.
- [15] J. M. Lopera, M.J. Prieto, A. M. Perna, and F. N. Nuno, "A multiwinding modeling method for high frequency transformers and inductors," *IEEE Trans. Power Electron.*, vol.18, no.3, May 2003.
- [16] A., Besri, X. Margueron, J.-P. Keradec, and B. Delinchant, "Wide frequency range lumped element equivalent circuit for HF planar transformer," *Proc. of the IEEE Power Electron. Special. Conf. (PESC)*, no., pp.766-772, 15-19 June 2008.
- [17] A.M. Pernia, F. Nuno, and J.M. Lopera, "1D/2D transformer electric model for simulation in power converters," *Proc. of the IEEE Power Electron. Special. Conf. (PESC)*, pp.1043-1049 vol.2, 18-22, Jun 1995.
- [18] R. Asensi, J. A. Cobos, O. Garcia, R. Prieto, and J. Uceda, "A full procedure to model high frequency transformer windings," *Proc. of the IEEE Power Electron. Special. Conf. (PESC)*, pp.856-863 vol.2, 20-25 Jun 1994.
- [19] P. G., Blanken, "A lumped winding model for use in transformer models for circuit simulation," *IEEE Trans. Power Electron.*, vol.16, no.3, pp. 445-460, May 2001.
- [20] X. Margueron, A. Besri, Y. Lembeye and J.-P. Keradec, "Current sharing between parallel turns of a planar transformer: prediction and improvement using a circuit simulation software," *IEEE Trans. on Ind. Applica.*, vol.46, no.3, May-June 2010.
- [21] C. R. Sullivan, "Optimal choice for number of strands in a Litz-wire transformer winding," *IEEE Trans. Power Electron.*, vol.14, no.2, pp.283-291, Mar 1999.
- [22] S. J. Gunter, K. K. Afridi, D. M. Otten, R. A. Abramson, and D. J. Perreault, "Impedance Control Network Resonant Step-Down DC-DC Converter Architecture," *Proc. of the IEEE Energy Conv. Congr. and Expo. (ECCE)*, Montreal, Canada, September 2015.
- [23] PL140 Series SMT Planar Transformers Datasheets [Online], Coilcraft, Inc., Available: <http://www.coilcraft.com/pdfs/pl140.pdf>.